Supporting Information

Robust Visible-light Photocatalytic H_2 Evolution of 2D RGO/$Cd_{0.15}Zn_{0.85}In_2S_4$-$Ni_2P$ Hierarchitectures

Haifeng Lin,[a] Xue Sui,[a] Jiakun Wu,[a] Qiqi Shi,[a] Hanchu Chen,[a,c] Hui Wang,*[a,c] Shaoxiang Li,[b] Yanyan Li,*[a] Lei Wang*[a,b] and Kam Chiu Tam*[d]

[a] *Key Laboratory of Eco-chemical Engineering, Key Laboratory of Optic-electric Sensing and Analytical Chemistry of Life Science, Taishan Scholar Advantage and Characteristic Discipline Team of Eco-Chemical Process and Technology, College of Chemistry and Molecular Engineering, Qingdao University of Science and Technology, Qingdao 266042, P. R. China*

[b] *Shandong Engineering Research Center for Marine Environment Corrosion and Safety Protection, College of Environment and Safety Engineering, Qingdao University of Science and Technology, Qingdao 266042, P. R. China*

[c] *Shandong Provincial Key Laboratory of Olefin Catalysis and Polymerization, Key Laboratory of Rubber-Plastics of Ministry of Education, School of Polymer Science and Engineering, Qingdao University of Science and Technology, Qingdao 266042, P. R. China*

[d] *Department of Chemical Engineering, Waterloo Institute for Nanotechnology, University of Waterloo, 200 University Avenue West, Waterloo, Ontario, N2L 3G1, Canada*

* Corresponding authors. E-mail addresses: h54wang@uwaterloo.ca, liyanyan6771@163.com, inorchemwl@126.com, mkctam@uwaterloo.ca.

Characterization results

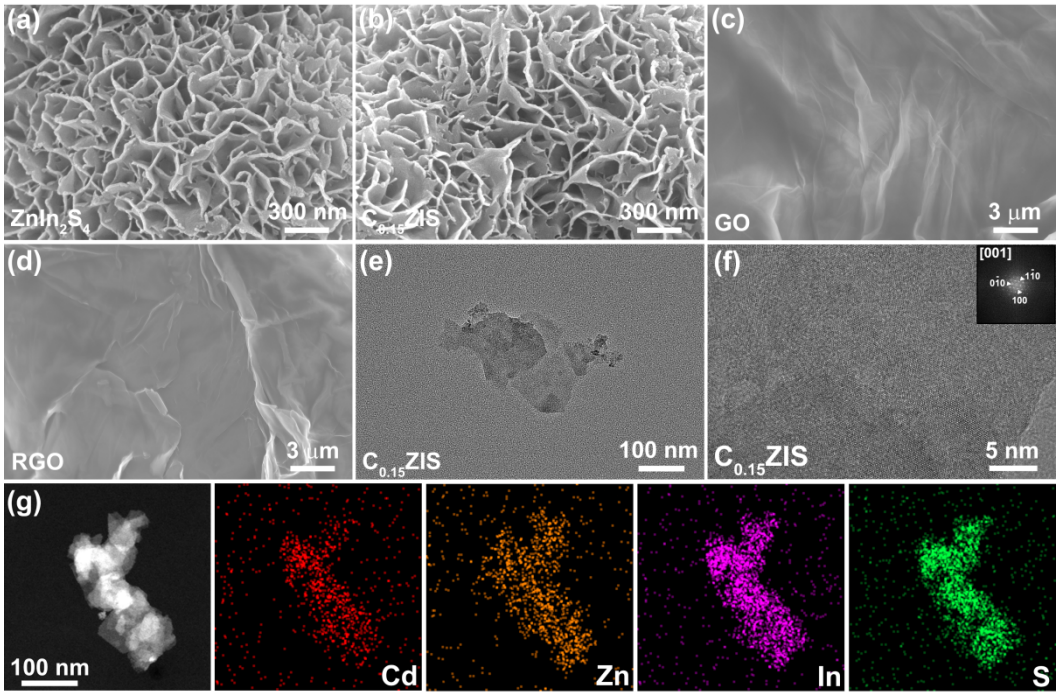

Fig. S1. (a-d) SEM images of (a) $ZnIn_2S_4$ nanosheets, (b) $C_{0.15}$ZIS nanosheets, (c) GO nanosheets, and (d) RGO nanosheets. (e) TEM, (f) HRTEM, and (g) STEM and EDX mapping results of $C_{0.15}$ZIS nanosheets.

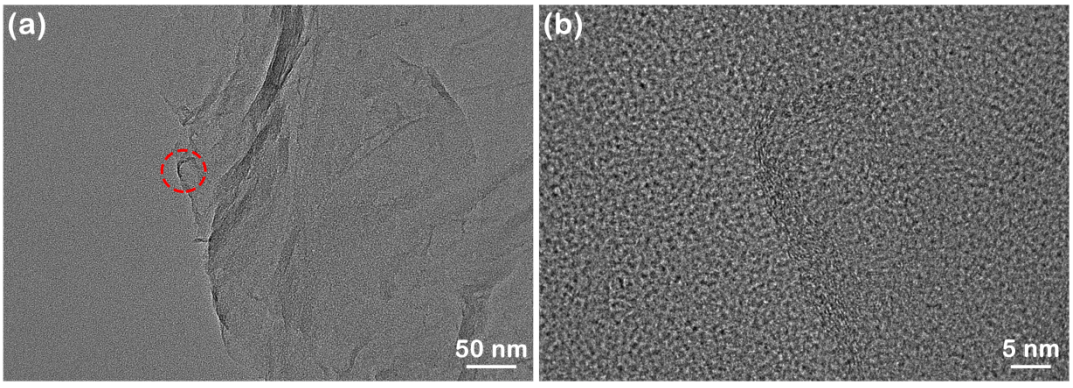

Fig. S2. (a) TEM and (b) HRTEM images of RGO nanosheets. (b) is magnified from the area (red dotted circle) marked in (a).

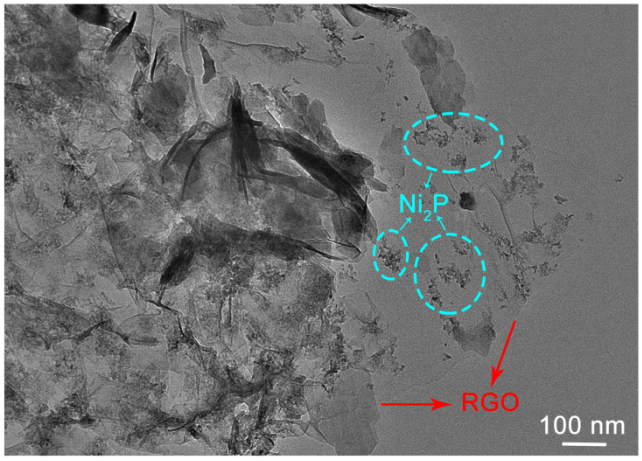

Fig. S3. TEM observation on the edge area of 2%-RGO/$C_{0.15}$ZIS-3N composite.

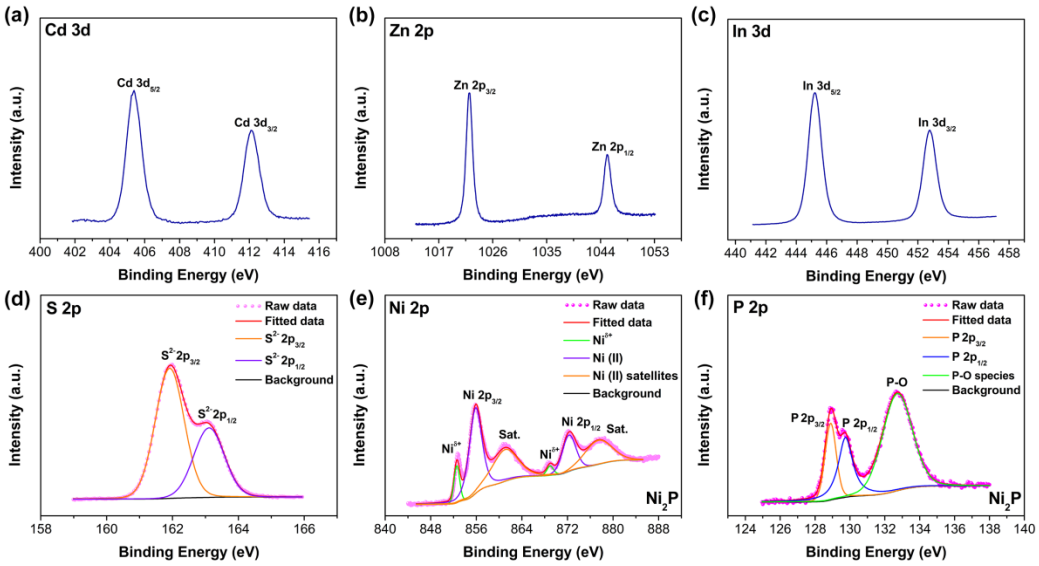

Fig. S4. (a) Cd 3d, (b) Zn 2p, (c) In 3d, and (d) S 2p XPS spectra of $C_{0.15}$ZIS nanosheets. (e) Ni 2p and (f) P 2p XPS spectra of Ni_2P nanoparticles.

Table S1. The mole ratios of C-C, C-OH, C-O-C, and C-OOH estimated from the C 1s spectra of different samples.

Sample	C-C (mole ratio)	C-OH (mole ratio)	C-O-C (mole ratio)	C-OOH (mole ratio)
GO	26.7%	10.2%	51.2%	11.9%
RGO	58.5%	24.7%	16.8%	0
fresh 2%-RGO/$C_{0.15}$ZIS	33.8%	31.2%	35.0%	0
used 2%-RGO/$C_{0.15}$ZIS	35.1%	29.1%	35.8%	0

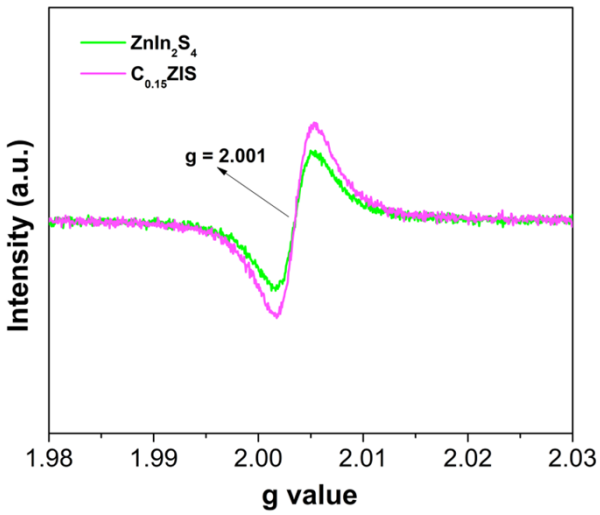

Fig. S5. EPR spectra of $ZnIn_2S_4$ and $C_{0.15}$ZIS nanosheets.

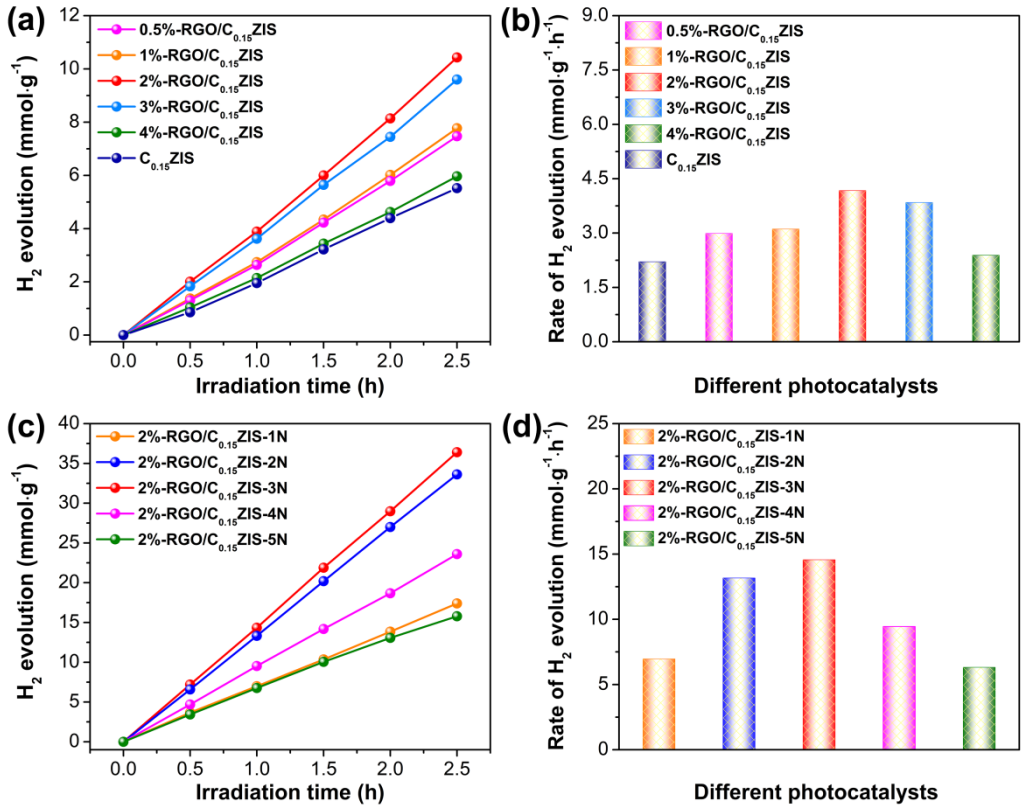

Fig. S6. (a, c) Photocatalytic H_2 generation activities and (b, d) corresponding HER rates of (a, b) x-RGO/$C_{0.15}$ZIS (x = 0, 0.5%, 1%, 2%, 3%, and 4%) and (c, d) 2%-RGO/$C_{0.15}$ZIS-yN (y = 1, 2, 3, 4, and 5).

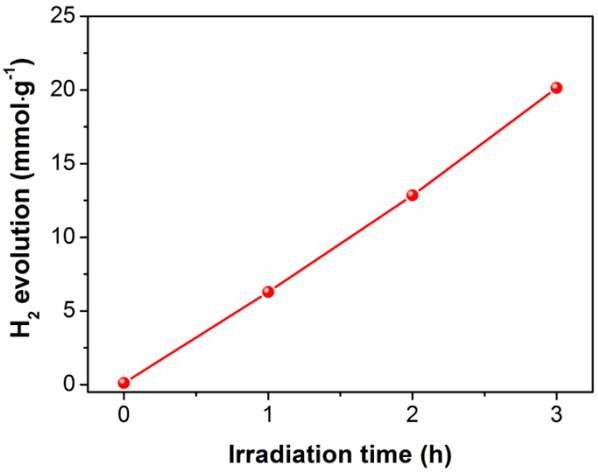

Fig. S7. H_2 evolution curve for calculating the AQY of 2%-RGO/$C_{0.15}$ZIS-3N.

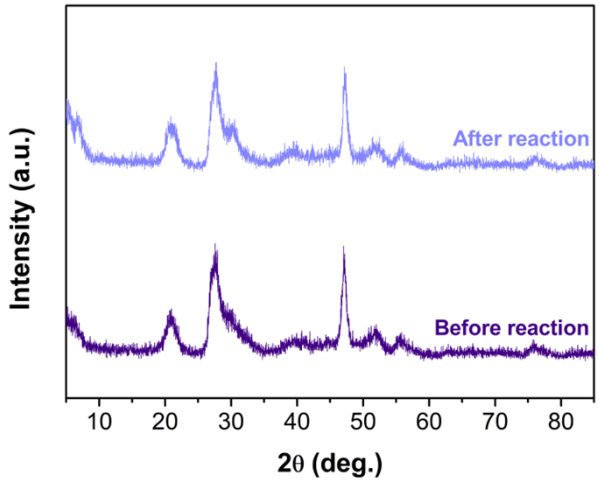

Fig. S8. XRD patterns of the 2%-RGO/$C_{0.15}$ZIS-3N hybrid before and after HER test.

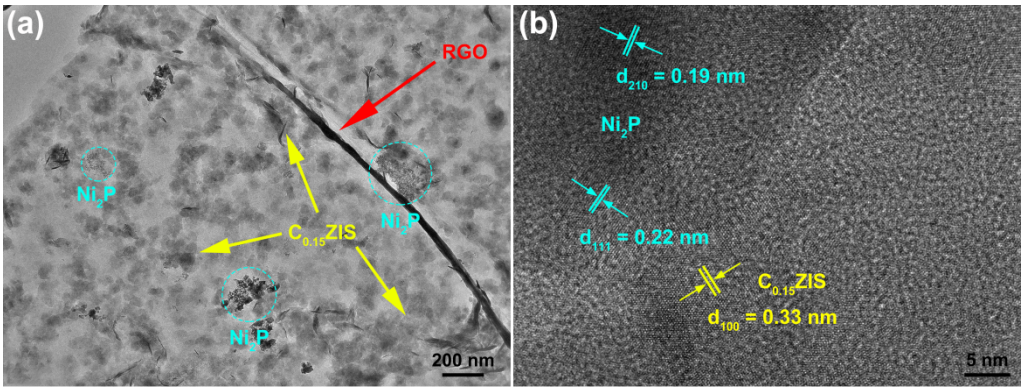

Fig. S9. (a) TEM and (b) HRTEM graphs of the 2%-RGO/$C_{0.15}$ZIS-3N composite after HER measurement.

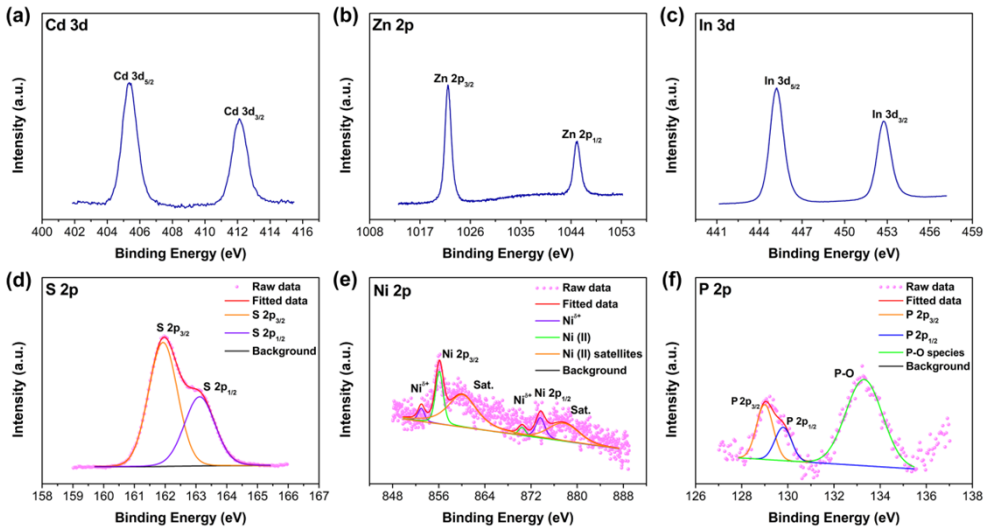

Fig. S10. (a) Cd 3d, (b) Zn 2p, (c) In 3d, (d) S 2p, (e) Ni 2p, and (f) P 2p spectra of 2%-RGO/$C_{0.15}$ZIS-5N after photocatalytic reaction.

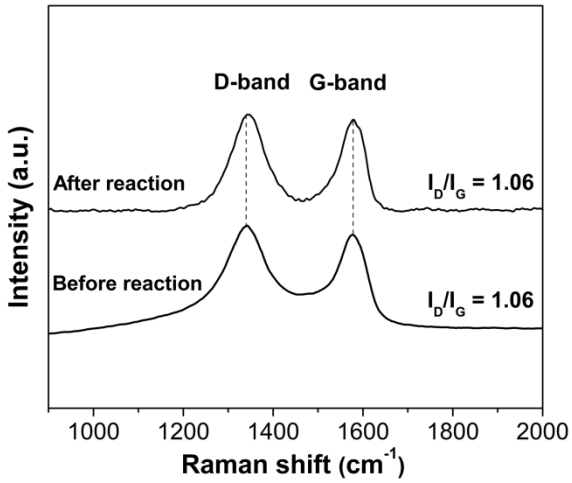

Fig. S11. Raman spectra of 2%-RGO/$C_{0.15}$ZIS before and after photocatalytic reaction.

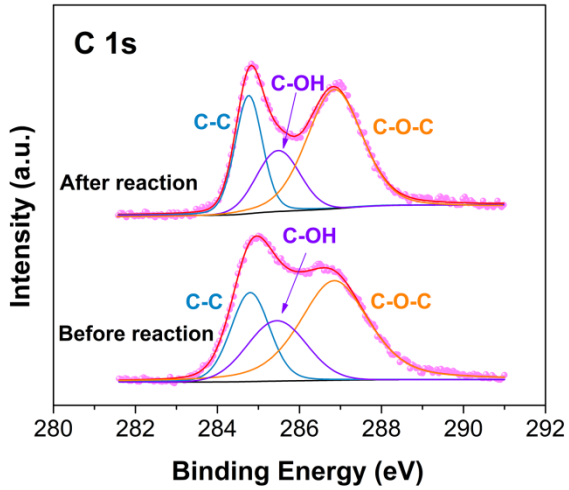

Fig. S12. C 1s signals of 2%-RGO/$C_{0.15}$ZIS before and after photocatalytic reaction.

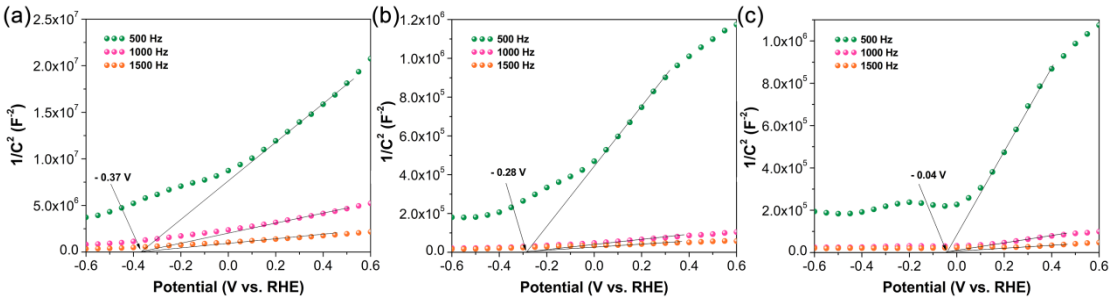

Fig. S13. Mott-Schottky curves of (a) $C_{0.15}$ZIS, (b) 2%-RGO/$C_{0.15}$ZIS, and (c) 2%-RGO/$C_{0.15}$ZIS-3N.

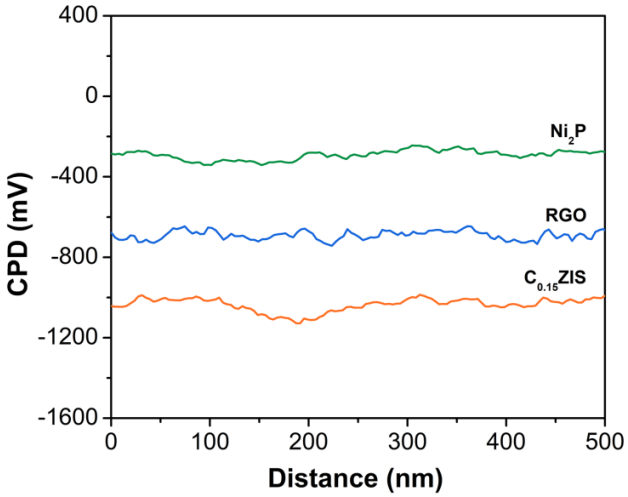

Fig. S14. Contact potential differences of Ni_2P, RGO, and $C_{0.15}$ZIS relative to the probe.

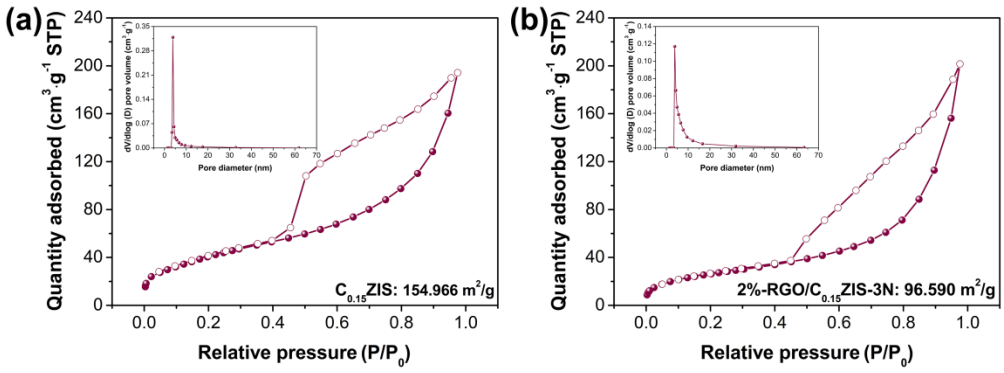

Fig. S15. N_2 adsorption-desorption isotherms and corresponding pore-size distributions of (a) $C_{0.15}$ZIS and (b) 2%-RGO/$C_{0.15}$ZIS-3N.

Table S2. Comparison on the photocatalytic HER activities of $ZnIn_2S_4$-based composites.

Photocatalyst	Hole scavenger (aqueous solution)	Light source (Xe lamp)	Maximum rate ($mmol \cdot h^{-1} \cdot g^{-1}$)	AQY (420 nm)	Reference
RGO/$C_{0.15}$ZIS-Ni_2P	lactic acid	λ > 400 nm	14.56	10.94% (400 nm)	This work
RGO/$ZnIn_2S_4$	lactic acid	λ > 420 nm	0.82	-	[1]
RGO/$ZnIn_2S_4$	TEOA	λ > 420 nm	2.64	4.4%	[2]
$ZnIn_2S_4$/RGO	TEOA	λ > 400 nm	5.06	-	[3]
Ag:$ZnIn_2S_4$/RGO	TEOA	λ > 420 nm	6.34	-	[4]
Cu_2Ni_1–$ZnIn_2S_4$	Na_2S/Na_2SO_3	λ > 420 nm	7.82	30.19%	[5]
Ni/$ZnIn_2S_4$-RV_s	TEOA	λ > 420 nm	1.79	9.6%	[6]
SnSe-$ZnIn_2S_4$	TEOA	λ > 400 nm	5.65	8.2%	[7]
Pd@UiO-66-NH_2@$ZnIn_2S_4$	TEOA	λ > 420 nm	5.26	3.2%	[8]
Li_xMoS_2/$ZnIn_2S_4$	Na_2S/Na_2SO_3	λ > 420 nm	6.65	-	[9]
$ZnIn_2S_4$ MFs	TEOA	λ > 420 nm	2.40	0.16%	[10]
Ag_2O-$ZnIn_2S_4$	TEOA	Simulated sunlight	0.46	0.9%	[11]
Co–P/$ZnIn_2S_4$	lactic acid	λ > 420 nm	7.84	4.3%	[12]
WS_2/$ZnIn_2S_4$	lactic acid	λ > 420 nm	2.55	3.2%	[13]
$CoFe_2O_4$/$ZnIn_2S_4$	TEOA	λ > 420 nm	0.8	5.0%	[14]
Au@Pt/$ZnIn_2S_4$	Na_2S/Na_2SO_3	λ > 420 nm	4.17	6.23%	[15]
Co_9S_8@$ZnIn_2S_4$@PdS	TEOA	λ > 420 nm	11.41	71.2%	[16]
$ZnIn_2S_4$/Nd	Na_2S/Na_2SO_3	λ > 420 nm	1.13	-	[17]
CeO_2/$ZnIn_2S_4$	Na_2S/Na_2SO_3	λ > 420 nm	0.85	-	[18]
$ZnIn_2S_4$@PCN-224	Na_2S/Na_2SO_3	λ > 420 nm	5.68	-	[19]
$Ti_3C_2T_X$ MXene@$ZnIn_2S_4$	TEOA	λ > 420 nm	3.47	11.14%	[20]
H-doped $ZnIn_2S_4$	Na_2S/Na_2SO_3	λ > 420 nm	2.15	13.2%	[21]
N-doped $ZnIn_2S_4$	TEOA	λ > 400 nm	11.08	13.8%	[22]
Oxygen-Doped $ZnIn_2S_4$	Na_2S/Na_2SO_3	λ > 420 nm	2.12	-	[23]

References:

[1] L. Ye, J. Fu, Z. Xu, R. Yuan, Z. Li, Facile One-Pot Solvothermal Method to Synthesize Sheet-on-Sheet Reduced Graphene Oxide (RGO)/$ZnIn_2S_4$ Nanocomposites with Superior Photocatalytic Performance, ACS Appl. Mater. Interfaces 6 (2014) 3483-3490.

[2] Y. Xia, Q. Li, K. Lv, D. Tang, M. Li, Superiority of graphene over carbon analogs for enhanced photocatalytic H_2-production activity of $ZnIn_2S_4$, Appl. Catal. B-Environ. 206 (2017) 344-352.

[3] C. Du, B. Yan, Z. Lin, G. Yang, Cross-linked bond accelerated interfacial charge transfer in

monolayer zinc indium sulfide ($ZnIn_2S_4$)/reduced graphene oxide (RGO) heterostructure for photocatalytic hydrogen production with mechanistic insight, Catal. Sci. Technol. 9 (2019) 4066-4076.

[4] Y. Gao, B. Xu, M. Cherif, H. Yu, Q. Zhang, F. Vidal, X. Wang, F. Ding, Y. Sun, D. Ma, Y. Bi, Z. Xu, Atomic insights for Ag Interstitial/Substitutional doping into $ZnIn_2S_4$ nanoplates and intimate coupling with reduced graphene oxide for enhanced photocatalytic hydrogen production by water splitting, Appl. Catal. B-Environ. 279 (2020) 119403.

[5] J. Jin, Y. Cao, T. Feng, Y. Li, R. Wang, K. Zhao, W. Wang, B. Dong, L. Cao, Constructing CuNi dual active sites on $ZnIn_2S_4$ for highly photocatalytic hydrogen evolution, Catal. Sci. Technol. 11 (2021) 2753-2761.

[6] J. Pan, G. Zhang, Z. Guan, Q. Zhao, G. Li, J. Yang, Q. Li, Z. Zou, Anchoring Ni single atoms on sulfur-vacancy-enriched $ZnIn_2S_4$ nanosheets for boosting photocatalytic hydrogen evolution, J. Energy Chem. 58 (2021) 408-414.

[7] C. Du, B. Yan, G. Yang, Promoting photocatalytic hydrogen evolution by introducing hot islands: SnSe nanoparticles on $ZnIn_2S_4$ monolayer, Chem. Eng. J. 404 (2021) 126477.

[8] M. Cao, F. Yang, Q. Zhang, J. Zhang, L. Zhang, L. Li, X. Wang, W.L. Dai, Facile construction of highly efficient MOF-based Pd@UiO-66-NH_2@$ZnIn_2S_4$ flower-like nanocomposites for visible-light-driven photocatalytic hydrogen production, J. Mater. Sci. Technol. 76 (2021) 189-199.

[9] J. Liu, W. Fang, Z. Wei, Z. Qin, Z. Jiang, W. Shangguan, Metallic 1T-Li_xMoS_2 co-catalyst enhanced photocatalytic hydrogen evolution over $ZnIn_2S_4$ floriated microspheres under visible light irradiation, Catal. Sci. Technol. 8 (2018) 1375-1382.

[10] X. Jing, N. Lu, J. Huang, P. Zhang, Z. Zhang, One-step hydrothermal synthesis of S-defect-controlled $ZnIn_2S_4$ microflowers with improved kinetics process of charge-carriers for photocatalytic H_2 evolution, J. Energy Chem. 58 (2021) 397-407.

[11] Y. Xiao, Z. Peng, W. Zhang, Y. Jiang, L. Ni, Self-assembly of Ag_2O quantum dots on the surface of $ZnIn_2S_4$ nanosheets to fabricate p-n heterojunctions with wonderful bifunctional photocatalytic performance, Appl. Surf. Sci. 494 (2019) 519-531.

[12] Q. Liu, M. Wang, Y. He, X. Wang, W. Su, Photochemical route for synthesizing Co-P alloy decorated $ZnIn_2S_4$ with enhanced photocatalytic H_2 production activity under visible light irradiation, Nanoscale 10 (2018) 19100-19106.

[13] M. Xiong, B. Chai, J. Yan, G. Fan, G. Song, Few-layer WS_2 decorating $ZnIn_2S_4$ with markedly promoted charge separation and photocatalytic H_2 evolution activity, Appl. Surf. Sci. 514 (2020) 145965.

[14] C. Li, H. Che, P. Huo, Y. Yan, C. Liu, H. Dong, Confinement of ultrasmall $CoFe_2O_4$ nanoparticles in hierarchical $ZnIn_2S_4$ microspheres with enhanced interfacial charge separation for photocatalytic H_2 evolution, J. Colloid Interf. Sci. 581 (2021) 764-773.

[15] H. An, Z. Lv, K. Zhang, C. Deng, H. Wang, Z. Xu, M. Wang, Z. Yin, Plasmonic coupling enhancement of core-shell Au@Pt assemblies on $ZnIn_2S_4$ nanosheets towards photocatalytic H_2 production, Appl. Surf. Sci. 536 (2021) 147934.

[16] M. Wang, G. Zhang, Z. Guan, J. Yang, Q. Li, Spatially Separating Redox Centers and Photothermal Effect Synergistically Boosting the Photocatalytic Hydrogen Evolution of $ZnIn_2S_4$ Nanosheets, Small 17 (2021) 2006952.

[17] R. Janani, G.S. Priyanga, S. Behara, A.A. Melvin, A.R.M. Shaheer, T. Thomas, B. Neppolian, S. Singh, Enhanced solar light driven hydrogen generation and environment remediation through Nd

incorporated $ZnIn_2S_4$, Renew. Energ. 162 (2020) 2031-2040.

[18] M. Zhang, J. Yao, M. Arif, B. Qiu, H. Yin, X. Liu, S.M. Chen, 0D/2D $CeO_2/ZnIn_2S_4$ Z-scheme heterojunction for visible-light-driven photocatalytic H_2 evolution, Appl. Surf. Sci. 526 (2020) 145749.

[19] P. Jin, L. Wang, X. Ma, R. Lian, J. Huang, H. She, M. Zhang, Q. Wang, Construction of hierarchical $ZnIn_2S_4$@PCN-224 heterojunction for boosting photocatalytic performance in hydrogen production and degradation of tetracycline hydrochloride, Appl. Catal. B-Environ. 284 (2021) 119762.

[20] G. Zuo, Y. Wang, W.L. Teo, A. Xie, Y. Guo, Y. Dai, W. Zhou, D. Jana, Q. Xian, W. Dong, Y. Zhao, Ultrathin $ZnIn_2S_4$ Nanosheets Anchored on $Ti_3C_2T_X$ MXene for Photocatalytic H_2 Evolution, Angew. Chem. Int. Edit. 59 (2020) 11287-11292.

[21] Y. Zhu, L. Wang, Y. Liu, L. Shao, X. Xia, In-situ hydrogenation engineering of $ZnIn_2S_4$ for promoted visible-light water splitting, Appl. Catal. B-Environ. 241 (2019) 483-490.

[22] C. Du, B. Yan, Z. Lin, G. Yang, Enhanced carrier separation and increased electron density in 2D heavily N-doped $ZnIn_2S_4$ for photocatalytic hydrogen production, J. Mater. Chem. A 8 (2020) 207-217.

[23] W. Yang, L. Zhang, J. Xie, X. Zhang, Q. Liu, T. Yao, S. Wei, Q. Zhang, Y. Xie, Enhanced Photoexcited Carrier Separation in Oxygen-Doped $ZnIn_2S_4$ Nanosheets for Hydrogen Evolution, Angew. Chem. Int. Edit. 55 (2016) 6716-6720.